# Fabrication and Characterisation of Tin Dioxide-Coated Gold Nanocomposites for Potential Use in Applications of Solar Steam Generation

# Tshepho Trevor Makgale<sup>1</sup>

https://orcid.org/0000-0002-4444-8881 u14007739@tuks.co.za

### Mmantsae Diale<sup>1</sup>

https://orcid.org/0000-0002-6035-6688 mmantsae.diale@up.ac.za

# Pannan I. Kyesmen<sup>1</sup>

https://orcid.org/0000-0002-1088-3543

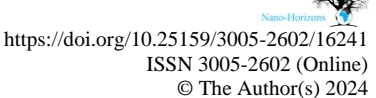
#### **Abstract**

In this study, we investigated the effects of coating gold (Au) nanostructures with metal oxide nanocrystalline solids and the impact this has on the properties of the Au-based nanofluids. We created nanofluids by combining ethylene glycol base fluid with tin dioxide-coated gold (Au@SnO<sub>2</sub>) nanocomposites. By encapsulating the Au nanostructures within SnO<sub>2</sub> nanocrystals, we were able to improve their structural stability and optical properties; this was confirmed by TEM micrographs and UV-Vis spectra. In addition, we found that the thermal conductivities of the Au@SnO<sub>2</sub>-based nanofluids were 10% higher than their uncoated counterparts. This suggests that the Au-based nanofluids composed of Au@SnO<sub>2</sub> nanocomposites have potential in thermal energy management and electronic cooling systems.

**Keywords:** Au@SnO<sub>2</sub>, nanocomposites, nanofluids, photo-absorption, photothermal materials, solar steam generator/generation.

1 Department of Physics, University of Pretoria, South Africa.







#### 1 Introduction

Solar energy is a form of clean and sustainable energy, and it presents new growth opportunities, with potential applications as diverse as solar power generation, photocatalysis, photothermal conversion and photovoltaic cells [1]. Solar thermal conversion technology, particularly solar steam generators (SSGs), is a promising technology with diverse applications, including water desalination and purification. SSGs are often composed of various materials, such as plasmonic metals and metal oxides [2], [3]. Recently, nanocomposites and nanohybrids of these materials have also been developed to improve efficiency [4].

Plasmonic metal nanomaterials such as Au, silver, platinum and copper are particularly useful in the conversion of light energy into thermal energy owing to their plasmonic properties and high thermal conductivity [5], [6]. These nanomaterials have high polarisable electron density that has interesting interactions with external radiation, which result in localised surface plasmon resonance (LSPR). The resulting electron oscillations, electron-electron scattering and electron redistribution contribute to the conversion of light energy to thermal energy. The heat generated is then transferred to the environment via phonon-phonon and electron-phonon coupling in the metal lattice, and results in solar steam generation when water molecules are carried to the photothermal layer and evaporated [7]. However, these metal nanomaterials possess narrow-band light absorptions and are unstable under high temperature conditions, which make them less useful in solar energy harvesting applications. Efforts are underway to broaden their light absorption band by modifying the particle size, composition or surrounding medium [8].

The aim of this study was to investigate the effects of modifying the surrounding medium of Au nanomaterials by coating them with tin dioxide (SnO<sub>2</sub>) nanocrystalline solids and to evaluate the resulting impact this has on the stability of the Au nanomaterials. The properties of nanofluids containing the tin dioxide-coated gold (Au@SnO<sub>2</sub>) nanocomposites were assessed with respect to light absorption, thermal conductivity and the potential use in the development of efficient thermal management systems.

# 2 Experimental Set-Up

The various types of Au nanostructure, such as gold nanospheres (Au-NSs) and gold nanoprisms (Au-NPRs), were synthesised using the seed-mediated growth procedures published by Zhou *et al.* [9] with a few modifications. The experimental set-up and implementation steps taken in synthesising the Au nanostructures are illustrated in Fig. 1.

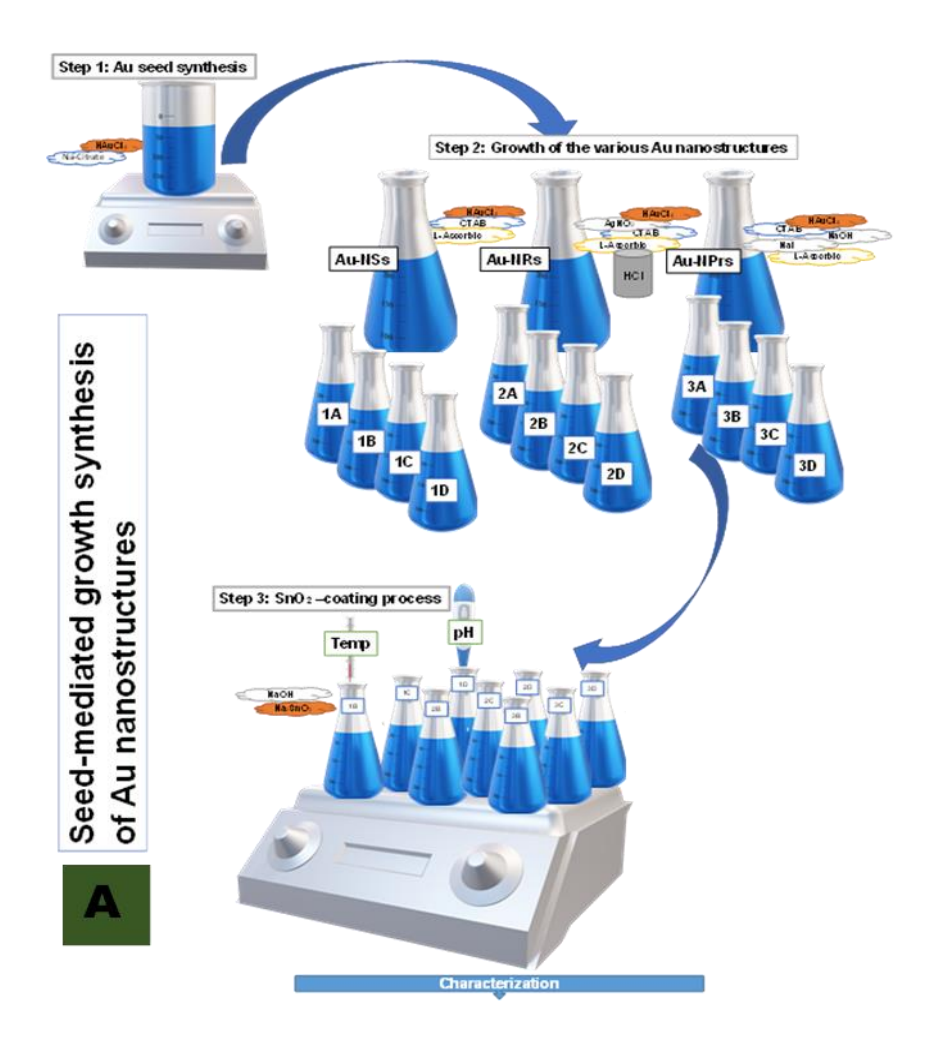


Fig. 1. Schematic representation of the synthesis of the Au-based nanofluids.

# Preparation of the Au-NSs

Three growth solution portions were prepared by combining HAuCl<sub>4</sub>, CTAB and L-ascorbic acid. The mixture was stirred and placed into separately labelled flasks. Auseed solution was added to each flask mixture and left overnight. The result was CTAB-capped Au-NSs.

### Preparation of the Au-NPRs

To prepare the growth solution, the following were sequentially mixed: 0.025 M CTAB solution, 0.02 M HAuCl<sub>4</sub> solution, 0.1 M NaOH solution, 0.1 M NaI solution and L-ascorbic acid solution. Glass beakers were used during the addition of Au-seeds to enable anisotropic growth. The mixture was left undisturbed overnight after turning

deep purple. Lastly, the resulting solution was divided into three portions and placed in separately labelled flasks.

# Preparation of the SnO<sub>2</sub>-Coated Au Nanostructures (Au@SnO<sub>2</sub>)

To prepare Au@SnO<sub>2</sub>, we followed the procedure of Zhou *et al.* [9] for forming SnO<sub>2</sub>-coated nanocomposite materials of Au-NSs and Au-NPRs. We diluted 5 ml of CTAB-capped Au-NSs and Au-NPRs samples to 20 ml with deionised water, adjusted the pH to 10.5, and heated the solutions to 75 °C for 15 min. We then added 3 ml of freshly prepared Na<sub>2</sub>SnO<sub>3</sub>·3H<sub>2</sub>O into each solution, stirred for 2 hours, and centrifuged the obtained Au@SnO<sub>2</sub> samples at 7 000 rpm, washed twice, and redispersed in 5 ml of deionised water.

#### **Characterisation of the Materials**

We used various characterisation techniques to evaluate the morphology, crystallinity, and optical properties of the Au nanomaterials and their nanocomposites. UV-Vis spectroscopic analyses were conducted to investigate the optical properties and colloidal stabilities, while the size and morphology properties of both SnO<sub>2</sub>-coated and uncoated Au nanostructures were determined using a JEOL FEGTEM-2100 FX transmission electron microscope, as illustrated in Fig. 2.

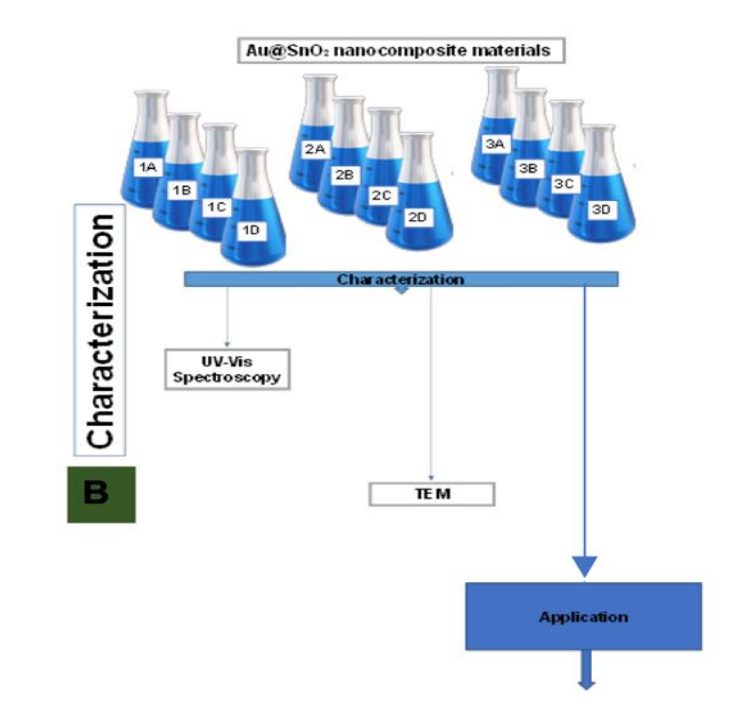


Fig. 2. Schematic representation of the characterisation of the Au-based nanofluid.

Fig. 3 shows the set-up of the transient hot-wire device, which includes a 10 cm platinum wire heat source with a diameter of 0.404 mm. This device was used to measure the thermal conductivity of Au-based nanofluids.

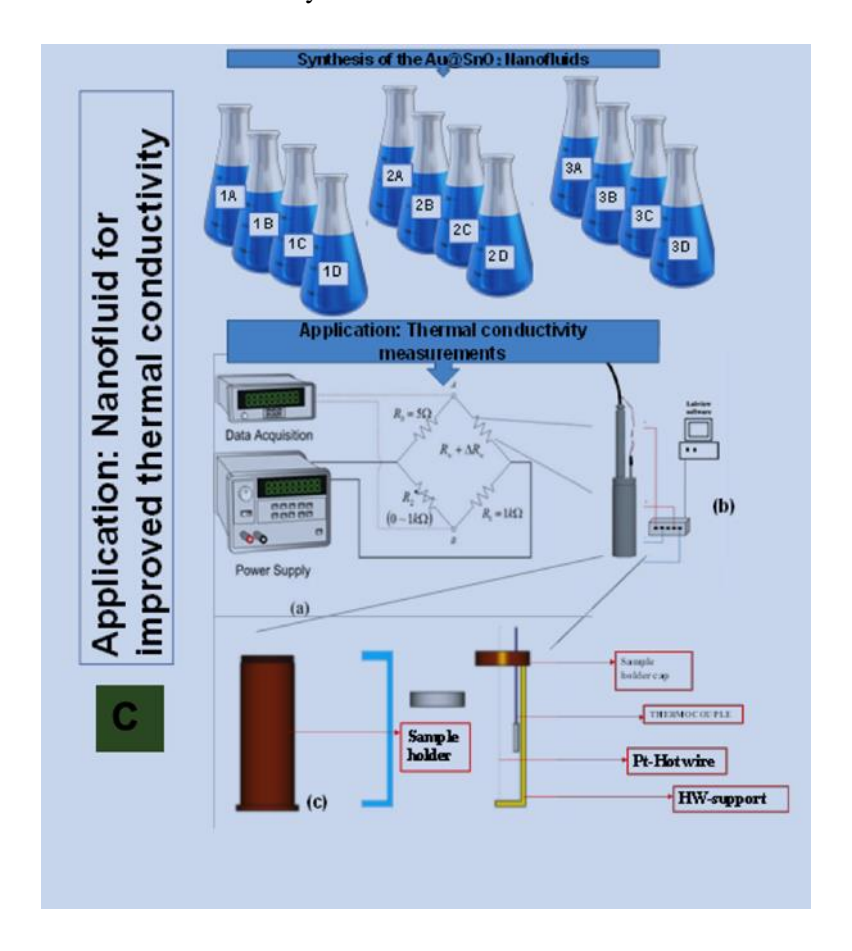


Fig. 3. Schematic representation of the application of the Au-based nanofluid.

### 3 Results and Discussion

# 3.1 Properties of the Au-NSs-Based Nanofluids

# 3.1.1 Optical Properties

Fig. 4 displays the optical absorption properties of two types of nanoparticles: CTAB-stabilised and SnO<sub>2</sub>-coated Au-NSs. The study aimed to determine the structural stability of Au-NSs by monitoring their optical properties over the course of three months. In the first month, the transverse surface plasmonic resonance band (SPRT) was observed at approximately 520 nm for CTAB-stabilised Au-NSs and approximately 530 nm for Au@SnO<sub>2</sub> solutions, consistent with previously reported values [9]. The

highest redshift was observed for the SnO<sub>2</sub>-coated sample. The red shift of the SPRT band for the coated particles was attributed to the high refractive index of SnO<sub>2</sub> coatings of (2.2) [10]. Remarkably, these SPRT positions and redshifts remained consistent for the second and third months. However, significant SPRT band broadening was observed for CTAB-stabilised Au-NSs in the third month. This was owing to the increasing size distributions of the particles, which resulted from their agglomeration.

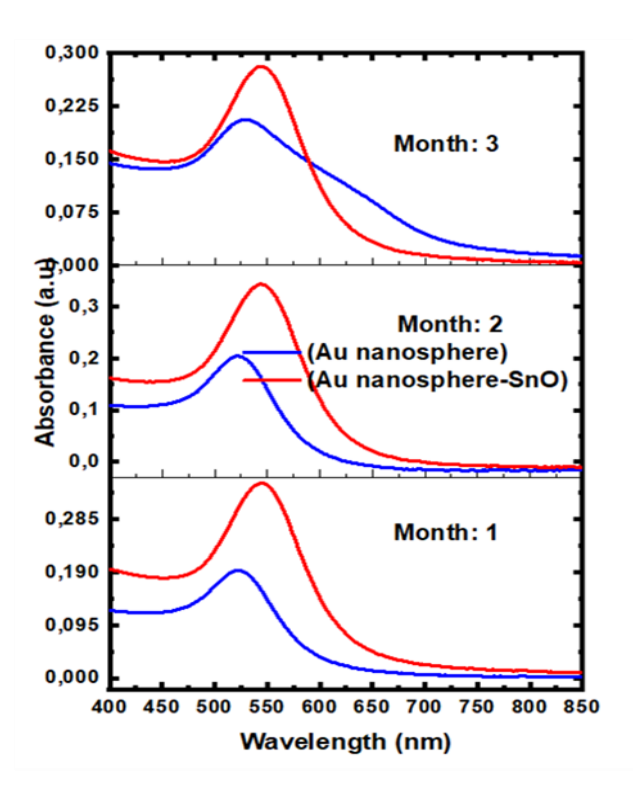


Fig. 4. Ultraviolet-visible spectroscopic graphs (UV-Vis spectra) for the CTAB-stabilised and SnO<sub>2</sub>-stabilised Au-NSs.

# 3.1.2 Morphological and Structural Properties

We studied the size and shape of Au-NSs using transmission electron microscopy (TEM). The TEM micrographs, shown in Fig. 5(A) to 5(C), were used to analyse CTAB-stabilised Au-NSs over three months. In the first month, well-dispersed and crystalline Au nano-spherical particles with an average size of less than 12 nm were observed as shown in Fig. 5(A). The optimised synthesis conditions led to pure spherical products with negligible amounts of by-products and a particle size distribution of  $\sim 12 \pm 24$  nm. In the second month, partially well-dispersed and crystalline Au nano-spherical particles with an average size of less than 31 nm were observed (Fig. 5(B)). A particle size distribution of  $\sim 31 \pm 32$  nm was obtained at this stage, with agglomerate products ranging from 20–30 nm in size. In the third month, mostly agglomerate

products with sizes more than 31 nm were observed (Fig. 5(C)). A particle size distribution of  $\sim 27 \pm 14$  nm was obtained after the synthesis.

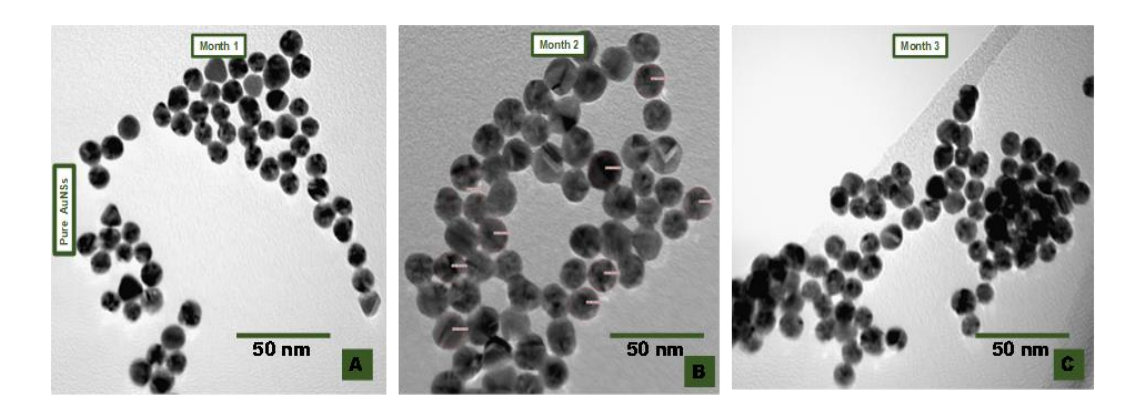


Fig. 5. The TEM micrographs of the CTAB-stabilised Au-NSs collected at various months after their initial synthesis.

In Fig. 6(A) to 6(C), we can see the TEM micrographs of the particles assumed to have the same size (approximately  $12 \pm 24$  nm) as the first month. Fig. 6(A) shows well-dispersed and crystalline Au nanospheres coated with SnO<sub>2</sub>, with an average coating thickness of less than 13 nm. This gives rise to average composite particle diameters of about 25 nm. Fig. 6(B) and 6(C) show the TEM micrographs collected in the second and third months, respectively. They reveal that the SnO<sub>2</sub>-stabilised nanomaterials were able to maintain their structural stability from month to month, unlike the CTAB-stabilised counterparts. In both micrographs, we can still see well-dispersed and crystalline Au nanospheres coated with SnO<sub>2</sub>. The average coating thickness sizes are less than 22.5 nm and 52 nm, which give rise to average composite particle diameters of about 34 nm and 64 nm, respectively.

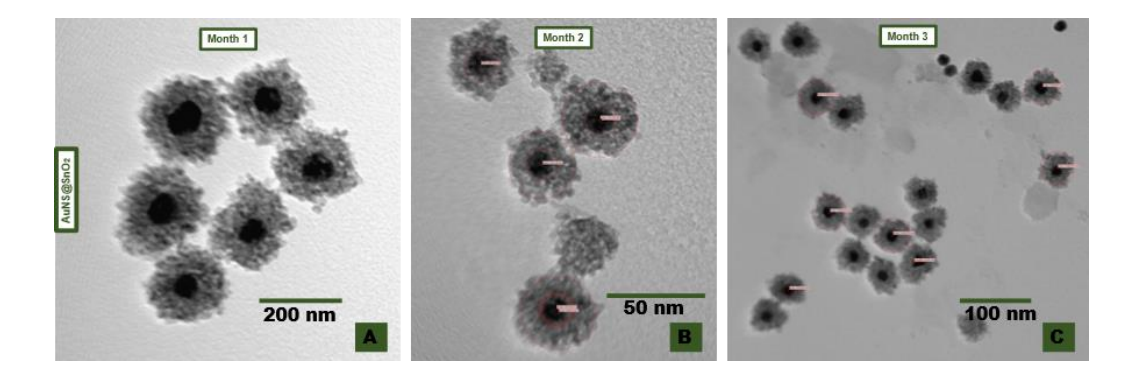


Fig. 6. The TEM of the SnO<sub>2</sub>-stabilised Au-NSs collected at various months after their initial synthesis.

We generated particle size histograms using ImageJ to determine the particle sizes. The concentric circles in the images only illustrate the different components in the nanocomposite materials.

## 3.1.3 Thermal Conductivity Properties

The nanofluids composed of the CTAB-stabilised and  $SnO_2$ -coated Au-NSs are shown in Fig. 7. The figure shows images of the samples after adding pure ethylene glycol to create  $\sim\!60\%$  EG+40%  $H_2O$  mixture solutions. Based on the literature-reported thermal conductivities given in Table I, it is expected that the base fluid will have a thermal conductivity of  $(0.502 \pm 0.384)$  W/mK [11].

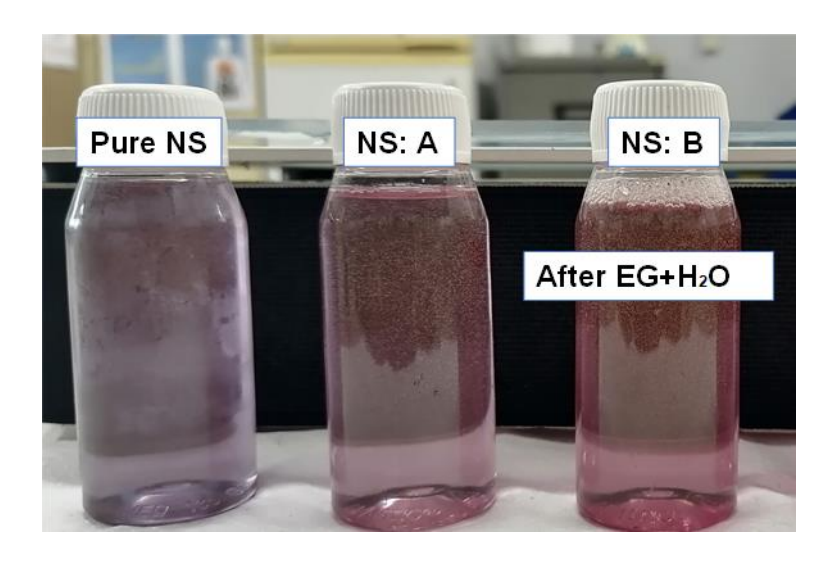


Fig. 7. The nanofluids composed of the CTAB-stabilised and SnO<sub>2</sub>-coated Au-NSs. Pure Au nanospheres (Pure NS), 5 mM concentrated SnO<sub>2</sub> around Au nanospheres (NS: A) and 10 mM concentrated SnO<sub>2</sub> around Au nanospheres (NS: B).

# TABLE I LITERATURE-REPORTED THERMAL CONDUCTIVITIES OF ETHYLENE GLYCOL MIXTURES WITH DISTILLED WATER [11]

Fluid	Thermal con	al conductivity	
	K (W m-1 K-1)	Std.	
Ethylene glycol + distilled water	0.502	0.384	
Ethylene glycol (J T Baker 99.90%) reported	0.256		
Distilled water (Q P) reported	0.609		

As shown in Fig. 8, the CTAB-stabilised Au-NSs have slightly similar thermal properties to the base fluid composed of a 60% EG-water mixture with a thermal conductivity of  $0.501 \pm 0.216$  W/mK. On the other hand, the SnO<sub>2</sub>-coated Au-NSs (NS: A) showed improved thermal properties with a thermal conductivity of  $1.242 \pm 0.955$  W/mK as expected. However, there was an unexpected result for the higher concentrated SnO<sub>2</sub>-coated Au-NSs of (NS: B) sample, with low thermal conductivity of  $0.105 \pm 0.072$  W/mK. This result may be attributable to excessive precipitation of Au@SnO<sub>2</sub> particles resulting from overcoating. In this case, the overcoat acts as a thermal shield.

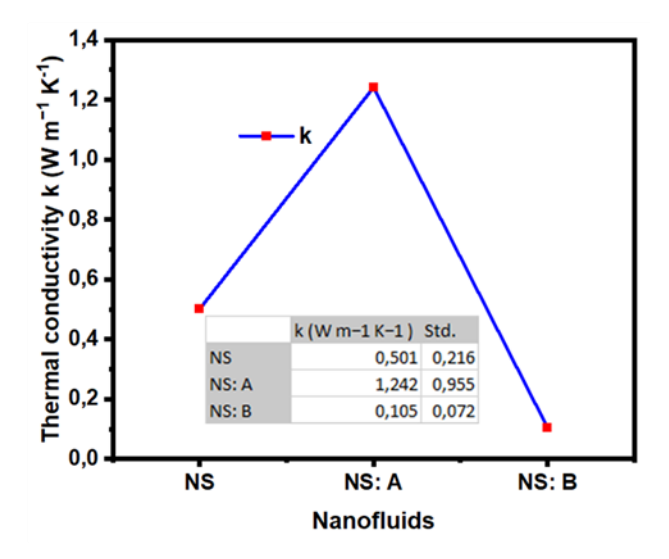


Fig. 8. The calculated thermal conductivities of the nanofluids composed of the CTAB-stabilised and SnO<sub>2</sub>-coated Au-NSs.

# 3.2 Properties of the Gold Nanoprims (Au-NPRs)-Based Nanofluids

# 3.2.1 Optical Properties

Fig. 9 illustrates the optical absorption properties of CTAB-stabilised and SnO<sub>2</sub>-coated Au nanoprisms (Au-NPRs). Our instrument only allowed us to observe the UV-VIS region, which revealed only the SPRT band at approximately 550 nm for CTAB-stabilised Au-NSs and approximately 575 nm for Au@SnO<sub>2</sub> solutions. These values align with previously reported values [9]. However, redshifts are observed for the SnO<sub>2</sub>-coated samples. The redshifts of the SPRT bands for the coated particles can be attributed to the high refractive index of SnO<sub>2</sub> coatings (2.2) [10]. The intensity of the absorption bands depends on the coating thickness for SnO<sub>2</sub>-coated Au-NPR samples, with the concentrated sample having the largest intensity.

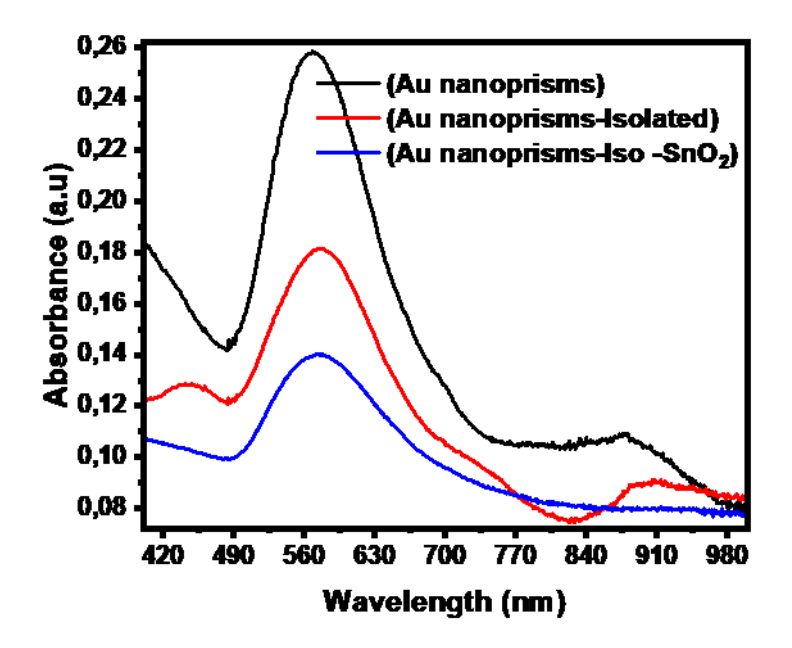
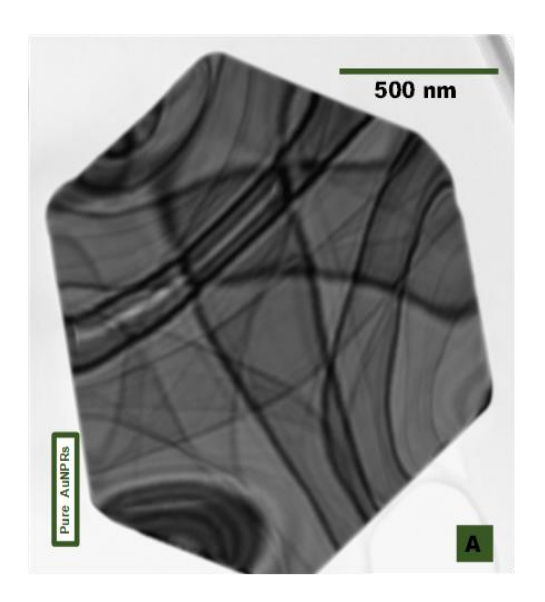


Fig. 9. Ultraviolet-visible spectroscopic graphs (UV-Vis spectra) for the CTABstabilised and SnO<sub>2</sub>-stabilised Au-NPRs.

### 3.2.2 Morphological and Structural Properties

In Fig. 10(A), a crystalline Au nanoprism with truncated vertices is revealed through a TEM micrograph. The nanomaterial has an average length of approximately 194 nm, and a particle size distribution of approximately  $194 \pm 201$  nm was obtained in the first month after the optimised synthesis conditions. This led to the synthesis of CTAB-stabilised nanoprism products with negligible amounts of by-products.

Fig. 10(B) displays the TEM micrograph of the  $SnO_2$ -coated gold nanoprisms (Au-NPRs@SnO<sub>2</sub>). All the particles in these micrographs are assumed to have the same particle diameter sizes as those used as the Au-seeds, which are ~12  $\pm$  24 nm in diameter and ~194  $\pm$  201 nm in length. As a result, Fig. 10(B) indicates the coating thickness of  $SnO_2$  around these Au-NPRs particles of approximately 68 nm, giving rise to an average composite particle length of approximately 262 nm. These thin film materials are inherently more stable than their spherical counterparts.



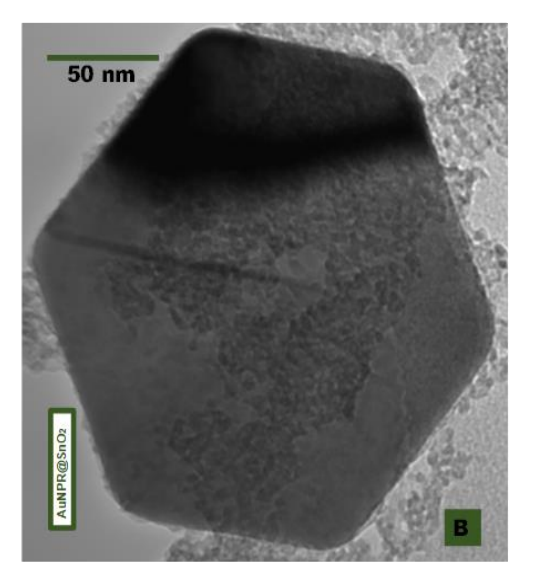


Fig. 10. The transmission electron micrographs (TEM) of the (A) CTAB-stabilised and (B) SnO<sub>2</sub>-stabilised Au-NPRs which were collected three months after their initial synthesis.

# 3.2.3 Thermal Conductivity Measurements

The nanofluids composed of the CTAB-stabilised and SnO<sub>2</sub>-coated Au-NPRs are shown in Fig. 11. The figure includes images of the samples after pure ethylene glycol was added to make the ~60% EG mixture solutions.

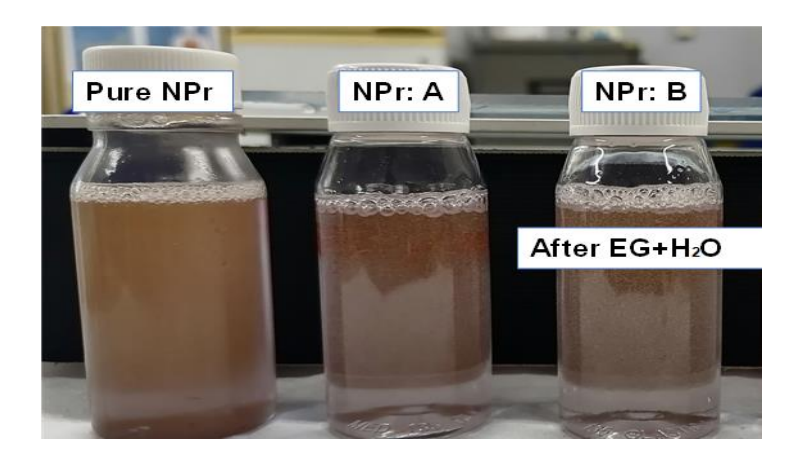


Fig. 11. The nanofluids composed of the CTAB-stabilised and SnO<sub>2</sub>-coated Au-NPRs. Pure Au nanoprisms (Pure NPr), 5 mM concentrated SnO<sub>2</sub> around Au nanoprisms (NPr: A) and 10 mM concentrated SnO<sub>2</sub> around Au nanoprisms (NPr: B).

In Fig. 12, it is evident that the thermal properties of Au-NPR nanomaterials, including CTAB-stabilised and SnO<sub>2</sub>-stabilised nanomaterials, are significantly lower than that of the base fluid, which is a 60% EG mixture. The CTAB-stabilised materials have a thermal conductivity of  $0.133 \pm 0.098$  W/mK, while the SnO<sub>2</sub>-coated Au-NPR sample (NPR: B) has a low thermal conductivity of  $0.110 \pm 0.092$  W/mK. However, the SnO<sub>2</sub>-coated Au-NRs (NR: A) have an improved thermal conductivity of  $0.462 \pm 0.366$  W/mK.

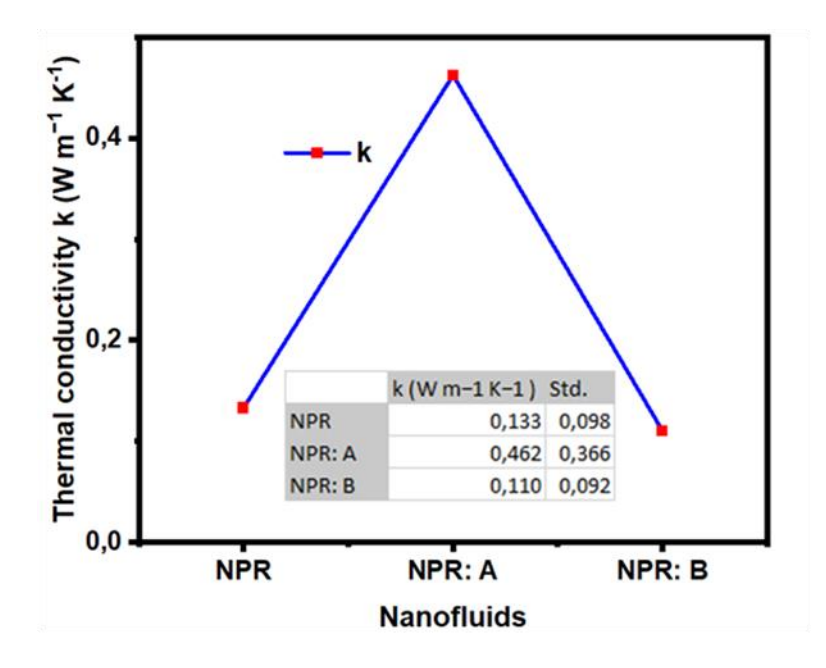


Fig. 12. The calculated thermal conductivities of the nanofluids composed of the CTAB-stabilised and SnO<sub>2</sub>-coated Au-NPRs.

#### 4 Conclusion

In our investigation of the effects of coating Au nanostructures with  $SnO_2$  nanocrystalline solids, we demonstrated that  $SnO_2$  has a stabilising effect on the core Au nanostructures. This was evidenced by their optical properties, which remained unchanged for several months after synthesis, unlike their uncoated counterparts. The impact of this coating on the properties of Au-based nanofluids showed mixed results. In some cases, it enhanced thermal conductivity, while in others it acted as an insulating barrier, which impeded heat transfer.

Interestingly, we identified the low thermal conductivity of CTAB-stabilised and SnO<sub>2</sub>-coated Au-NPRs as ideal for solar steam generation. Our findings also highlight that a high surface area alone is insufficient to guarantee high thermal conductivity. Effective

heat localisation is driven by factors such as phonon scattering, interfaces, boundaries and the porosity of the Au-NPRs. Notably, our research demonstrated significant improvements in optical light absorption, making these systems suitable as narrow-band absorbing agents in a composite absorber device.

# 5 References

- [1] K. K. Jaiswal *et al.*, "Renewable and sustainable clean energy development and impact on social, economic, and environmental health," *Energy Nexus*, vol. 7, Sept. 2022, doi: 10.1016/j.nexus.2022.100118.
- [2] I. Ibrahim, D. H. Seo, A. M. McDonagh, H. K. Shon and L. Tijing, "Semiconductor photothermal materials enabling efficient solar steam generation toward desalination and wastewater treatment," *Desalination*, vol. 500, Mar. 2021, doi: 10.1016/j.desal.2020.114853.
- [3] A. Mittal, R. Brajpuriya and R. Gupta, "Solar steam generation using hybrid nanomaterials to address global environmental pollution and water shortage crisis," *Mater. Today Sustain.*, vol. 21, Mar. 2023, doi: 10.1016/j.mtsust.2023.100319.
- [4] M. S. Asghar, N. Arshad, J. Tao, M. S. Irshad, J. Li and X. Wang, "Recent advances in multifunctional photothermal materials for solar-driven steam and energy generation," *Energy Technol.*, vol. 22, no. 9, Sept. 2023, doi: 10.1002/ente.202300500.
- [5] A. R. Indhu, L. Keerthana and G. Dharmalingam, "Plasmonic nanotechnology for photothermal applications – An evaluation," *Beilstein J. Nanotechnol.*, vol. 14, pp. 380– 419, Mar. 2023, doi: 10.3762/bjnano.14.33.
- [6] Z. Fattahi, A. Y. Khosroushahi and M. Hasanzadeh, "Recent progress on developing of plasmon biosensing of tumor biomarkers: Efficient method towards early stage recognition of cancer," *Biomed. Pharmacother.*, vol. 132, p. 110850, Dec. 2020, doi: 10.1016/j.biopha.2020.110850.
- [7] D. Dragoman, "Nanomaterials for energy harvesting," *Nanomaterials*, vol. 13, no. 7, p. 1154, Mar. 2023, doi: 10.3390/nano13071154.
- [8] C. Fei Guo, T. Sun, Q. Liu and Z. Ren, "Metallic nanostructures for light trapping in energy-harvesting devices," *Light Sci. Appl.*, vol. 3, p. e161, 2014, doi: 10.1038/lsa.2014.42.
- [9] N. Zhou, C. Ye, L. Polavarapu and Q-H. Xu, "Controlled preparation of Au/Ag/SnO<sub>2</sub> coreshell nanoparticles using a photochemical method and applications in LSPR based sensing," *Nanoscale*, vol. 7, no. 19, pp. 9025–9032, 2015, doi: 10.1039/C5NR01579K.

- [10] S. H. Lee, I. Rusakova, D. M. Hoffman, A. J. Jacobson and T. R. Lee, "Monodisperse SnO<sub>2</sub>-coated gold nanoparticles are markedly more stable than analogous SiO<sub>2</sub>-coated gold nanoparticles," *ACS Appl. Mater. Interfaces*, vol. 5, no. 7, pp. 2479–2848, Mar. 2013, doi: 10.1021/am302740z.
- [11] h2xengineering. "Glycol in heating and cooling systems What are the implications?" https://www.h2xengineering.com/blogs/glycol-in-heating-and-cooling-systems/ (accessed 19 November 2024).